Modulated Fluorite-Type Structure of Materials from the $(1-x)Y_{0.5}Zr_{0.5}O_{1.75}-xY_{0.75}Nb_{0.25}O_{1.75}$ ($0 \leq x \leq 1$) System

S. García-Martín,*,† M. A. Alario-Franco,† D. P. Fagg,‡ A. J. Feighery,‡ and J. T. S. Irvine‡

Departamento de Química Inorgánica, Facultad de Ciencias Químicas, Universidad Complutense de Madrid, Madrid-28040, Spain, and School of Chemistry, University of St. Andrews, St. Andrews, Fife KY16 9ST, United Kingdom

Received January 11, 2000

The microstructures of different high-temperature prepared oxides of the $(1-x)Y_{0.5}Zr_{0.5}O_{1.75}-xY_{0.75}Nb_{0.25}O_{1.75}$ ($0 \leq x \leq 1$) system have been studied by selected-area electron diffraction and high-resolution transmission electron microscopy. The materials show a modulated fluorite-type structure mainly due to a partial or short-range ordering of the oxygen vacancies. The modulation is related to the pyrochlore-type structure in the $Y_{0.75}Nb_{0.25}O_{1.75}$. A short-range ordering of the oxygen vacancies related to the C-type structure is observed in the $Y_{0.5}Zr_{0.5}O_{1.75}$. Gradual transition from the pyrochlore to the C-type structures is established with the variation of the composition.

Introduction

Pure ZrO_2 presents three different crystallographic polymorphs (monoclinic, tetragonal, and cubic) depending on the temperature. The highest temperature cubic polymorph can be stabilized by the addition of oxides of lower valent metals such as CaO, MgO, or lanthanide sesquioxides Ln_2O_3 and quenching from elevated temperatures (∼1600 °C). These substitutions create vacancies in the anion network to maintain electrical neutrality. The crystal structure has previously been described as "F-type" or "defect fluorite type", which implies no metal atom or anion vacancy ordering; also the composition range of the cubic solid solution depends on the nature of the aliovalent cation.

Defect fluorite type oxides are probably the most important kind of oxygen ion conductors and are involved in an increasing number of applications. Anion mobility is strongly dependent upon interaction or ordering of the oxygen vacancies and hence, structural studies on these materials are important to understand their physical properties.

It is well-known that many oxygen-deficient systems containing zirconia or hafnia have large regions of solid solution with "F-type" structure. At certain compositions and temperatures, however, vacancy and/or cation ordering occurs, giving rise to new structures, most of them related to the fluorite-type. Thus, the $Ca_xHf_{1-x}O_{2-x}$ system shows oxygen-vacancy ordering below 1700 K and at least three ordered phases: Ø, $Ø_1$, and $Ø_2$ corresponding to $x = 0.22$, 0.2, and 0.24 have been identified.[1−3] Nevertheless, even in the high-temperature disordered phases of these systems, apart from the characteristic reflections of the fluorite-type lattice, additional weak reflections and diffuse intensity features have been observed in their electron diffraction patterns. These data have been interpreted as microdomains of an ordered phase coherently intergrown within a cubic fluorite matrix.[4,5] This observation seems to be quite general because studies by single-crystal X-ray diffraction, powder and single-crystal neutron diffraction and electron diffraction have also revealed diffuse scattering in other high-temperature oxygen-deficient compounds belonging to systems with fluorite-related structures as, for instance, $ZrO_2-YO_{1.5}$,[6−8] $ZrO_2-LnO_{1.5}$ (Ln = Tb, Gd),[9] $UO_2-YO_{1.5}$,[10] and $UO_2-LaO_{1.5}$.[11] The phenomena has traditionally been interpreted in terms of small microdomains of ordered phases embedded within a fluorite matrix; the ordered phases imply oxygen-vacancy ordering or displacements of the ions (oxygen and cations) away from their regular fluorite lattice sites. Therefore, it is generally agreed that the concept of perfect disorder in these "defect fluorite" materials is not strictly correct.

* Author to whom inquiries about the paper may be addressed: Susana García-Martín, Departamento de Química Inorgánica, Facultad de Ciencias Químicas, Universidad Complutense de Madrid, Madrid-28040, Spain. Telephone: 91-394214. Fax: 91-3944352. E-mail: sgmartin@eucmax.sim.ucm.es.

† Universidad Complutense de Madrid.

‡ University of St. Andrews.

(1) Allpress, J. G.; Rossel, H. J.; Scott, H. G. *Mater. Res. Bull.* **1974**, *9*, 455.
(2) Rossel, H. J.; Scott, H. G. *J. Solid State Chem.* **1975**, *13*, 345.
(3) Allpress, J. G.; Rossel, H. J.; Scott, H. G. *J. Solid State Chem.* **1975**, *14*, 264.
(4) Allpress, J. G.; Rossel, H. J. *J. Solid State Chem.* **1975**, *15*, 68.
(5) Rossel, H. J.; Sellar, J. R.; Wilson, I. *J. Acta Crystallogr. B* **1991**, *47*, 862.
(6) Horiuchi, H.; Schultz, A. J.; Leung, P. C. W.; Williams, J. M. *Acta Crystallogr. B* **1984**, *40*, 367.
(7) Goff, J. P.; Hayes, W.; Hull, S.; Hutchings, M. T.; Clausen, K. N. *Phys. Rev. B* **1999**, *59*(22), 14202.
(8) Gibson, I. R.; Irvine, J. T. S. *J. Mater. Chem.* **1996**, *6*, 895.
(9) van Dijk, M. P.; Mijlhoff F. C.; Burggraaf, H. J. *J. Solid State Chem.* **1986**, *62*, 377.
(10) Pienkowski, M. C.; Jenkins, M. L.; Moseley, P. T. *J. Solid State Chem.* **1991**, *92*, 543.
(11) García-Chain, P.; Rojas, R. M.; Herrero, P.; Günter, J. R. *J. Solid State Chem.* **1994**, *108*, 236.

10.1021/cm991204l CCC: $19.00
Published on Web 05/06/2000

With regard to the applications of the oxygen-deficient fluorite-type oxides, most current research has focused on the use of these materials as components of solid oxide fuel cells (SOFC), in particular in designs based on the yttria-stabilized zirconia electrolyte with Ni/ZrO_2 cermets as anode. However, alternative anode materials are needed due to the operating problems associated with the Ni cermet compounds. Great attention has been centered on the materials of the $ZrO_2-YO_{1.5}-MO_x$ (M = transition metal) systems which present mixed ionic and (under reducing conditions) electronic conductivity, for being good candidates as anodes in SOFC. We have investigated the $ZrO_2-YO_{1.5}-NbO_{2.5}$ system[12−15] and found that these materials present a complex electrical behavior, which might be related to the local arrangement of the oxygen vacancies within their crystal structure. In the $(1-x)Y_{0.5}Zr_{0.5}O_{1.75}-xY_{0.75}Nb_{0.25}O_{1.75}$ ($0 \le x \le 1$) oxides, the ionic conductivity decreases with increasing yttrium and niobium content which means that other factors than the oxygen-vacancy concentration (which, in fact, here remains constant) determine the ionic conduction. Their detailed crystal structure is probably closely correlated to the electrical properties of these materials.

The aim of this work is to study the microstructure of high-temperature prepared materials of the $(1-x)Y_{0.5}Zr_{0.5}O_{1.75}-xY_{0.75}Nb_{0.25}O_{1.75}$ ($0 \le x \le 1$) system by selected-area electron diffraction (SAED) and high-resolution transmission electron microscopy (HRTEM) with the purpose of relating their physical properties with their crystal structure.

Experimental Section

Different compositions of the $(1-x)Y_{0.5}Zr_{0.5}O_{1.75}-xY_{0.75}Nb_{0.25}O_{1.75}$ ($0 \le x \le 1$) oxides were prepared from stoichiometric amounts of ZrO_2, Y_2O_3 and Nb_2O_5 ground under acetone using an agate pestle and mortar and dry pressed into pellets under a pressure of 3 tonnes/cm^2. Prior to weighing, it was necessary to dry Y_2O_3 for 24 h at 1000 °C to remove moisture and absorbed gases; ZrO_2 and Nb_2O_5 powders were dried at 700 °C for 24 h. Samples were fired in air at 1450−1500 °C for periods of 48−72 h with intermediate grinding and repressing until single-phase fluorite was achieved. Samples were rapidly cooled by removing from the furnace in alumina crucibles, which due to the refractory nature of these oxides effectively quenched their high-temperature structure to ambient.

Crystalline phase identification and determination of the lattice parameters were carried out by powder X-ray diffraction using a Stoe Stadi-P diffractometer with a position sensitive detector (PSD), Ge monochromator, and Cu Kα1 radiation.

For transmission electron microscopy the samples were ground in *n*-butyl alcohol and ultrasonically dispersed. A few drops of the resulting suspension were deposited in a carbon-coated grid. SAED studies were performed with an electron microscope JEOL 2000FX (double tilt ±45°) working at 200 kV and HRTEM studies with an electron microscope JEOL 4000FX (double tilt ±25°) working at 400 kV.

Results and Discussion

Powder XRD patterns of all the materials of the $(1-x)Y_{0.5}Zr_{0.5}O_{1.75}-xY_{0.75}Nb_{0.25}O_{1.75}$ ($0 \le x \le 1$) system indicate pure phases with "defect fluorite" type structure. Unit cell parameters of the solid solution show a strong dependence upon yttrium content, with a linear increase of unit cell edge with extent of substitution as might be expected from ionic radius considerations.

Figure 1 shows SAED patterns along different zone axis of $Y_{0.75}Nb_{0.25}O_{1.75}$. In addition to the sharp Bragg reflections consistent with a fluorite-type structure, very peculiar scattering distributions are observed in all the patterns.

$Y_{0.75}Nb_{0.25}O_{1.75}$ has been studied before also by means of electron diffraction and high-resolution transmission electron microscopy. Allpress and Rossel[16] explained the SAED patterns as due to the formation of microdomains of a superstructure existing in several orientations and coherent with a fluorite-type matrix but they did not describe the superstructure. Miida et al.[17] interpreted their own results as two-dimensional antiphase domains of a compositional and displacive modulated structure along the $[11\bar{2}]_f$ direction (f refers to the cubic fluorite structure).

Diffuse intensity is characteristic of modulated structures due to periodic perturbations (or modulations) of the basic cell. A modulated structure formalism seems to be well suited to the structural description of the high-temperature quenched $Y_{0.75}Nb_{0.25}O_{1.75}$: the diffuse scattering occurring at any position in reciprocal space is defined by a wave vector $G_F \pm q$, where G_F is a reciprocal lattice vector of the fluorite-type lattice and q is a modulation vector. We will now describe the patterns of Figure 1 using this modulated structure approach to have an idea of the 3D shape of the diffuse scattering in the reciprocal space.

Two satellite reflections at both sides of $G_F \pm {}^1/_2(111)^*$ positions can be observed in the pattern along the $[\bar{1}\bar{1}0]_f$ zone axis (Figure 1a). Tilting experiments show that these satellite reflections are indeed part of a ring of diffuse intensity with normal axis parallel to the $[1\bar{1}1]_f$ directions (see for instance the pattern along the $[3\bar{3}2]_f$ zone axis). Weak diffuse scattering appears at $G_F \pm (010)^*$, $G_F \pm (100)^*$ and very weak diffuse rings at $G_F \pm {}^1/_2(220)^*$ in the pattern along the $[001]_f$ zone axis (Figure 1b), although reflections of the type $G_F \pm (001)^*$ and $G_F \pm {}^1/_2(220)^*$ are extremely weak, almost imperceptible in the pattern corresponding to the $[\bar{1}\bar{1}0]_f$ axis. Diffuse rings centered around $G_F \pm {}^1/_2(3\bar{1}1)^*$ can also be seen in the pattern along the $[\bar{1}\bar{1}2]_f$ zone axis (Figure 1c); the two reflections which are part of a ring centered at around $G_F \pm {}^1/_2(111)^*$ are also observed and the weak reflections at $G_F \pm {}^1/_2(2\bar{2}0)^*$ are again almost imperceptible. The pattern corresponding to the $[10\bar{3}]_f$ zone axis, (Figure 1d), shows two satellite reflections around $G_F \pm {}^1/_2(311)^*$ (which are part of the ring centered at this position and well observed in the pattern along the $[\bar{1}\bar{1}2]_f$ axis) and the very weak intensity distribution at $G_F \pm (010)^*$. In the pattern along the $[3\bar{3}2]_f$ zone axis, (Figure 1e) diffuse rings are centered at $G_F \pm {}^1/_2(\bar{1}13)$, two reflections are located at both sides of $G_F \pm {}^1/_2(133)$ as part of a ring and very weak intensity at $G_F \pm {}^1/_2(220)^*$, and weak diffuse scattering distribution

(12) Irvine, J. T. S.; Gibson, I. R.; Fagg, D. P. *Ionics* **1995**, *1*, 279.
(13) Irvine, J. T. S.; Fagg, D. P.; Labrincha, J.; Marques, F. M. B. *Catalysis Today* **1997**, *38*, 467.
(14) Fagg, D. P.; Irvine, J. T. S. *Ionics* **1998**, *4*, 61.
(15) Irvine, J. T. S.; Feighery, A. J.; Fagg, D. P.; García-Martín, S. *Solid State Ionics*, in press.
(16) Allpress, J. G.; Rossel, H. J. *J. Solid State Chem.* **1979**, *27*, 105.
(17) Miida, R.; Sato, F.; Tanaka, M.; Naito, H.; Arashi, H. *J. Appl. Crystallogr.* **1997**, *30*, 272.

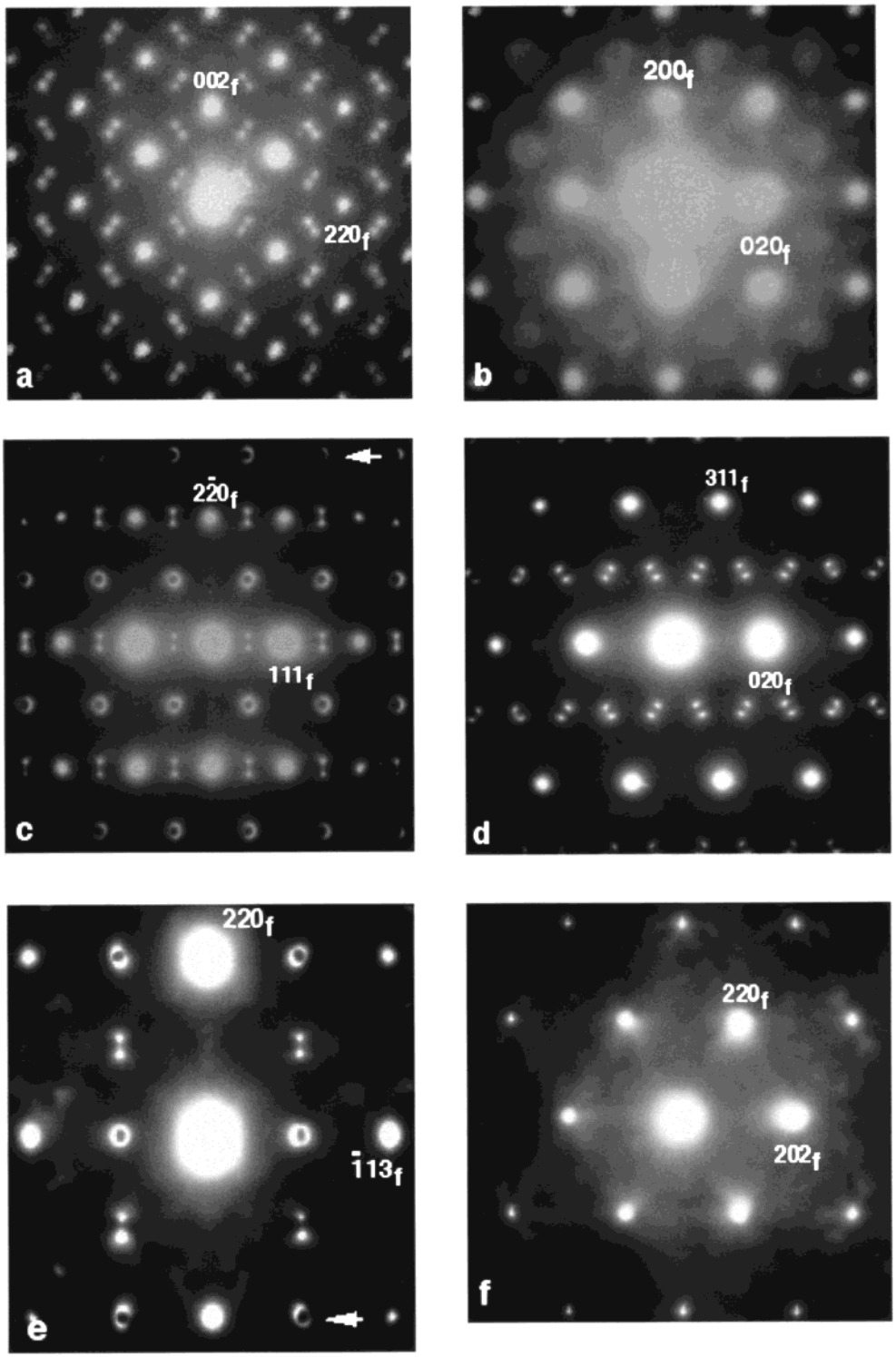

Figure 1. SAED patterns of $Y_{0.75}Nb_{0.25}O_{1.75}$ along the $[\bar{1}\bar{1}0]_f$ (a), $[001]_f$ (b), $[\bar{1}\bar{1}2]_f$ (c), $[10\bar{3}]_f$ (d), $[3\bar{3}2]_f$ (e) and $[1\bar{1}\bar{1}]_f$ (f) zone axes.

connecting the main reflections with the rings is observed. Weak diffuse intensity distribution connecting the main reflections is also seen in the pattern along the $[1\bar{1}\bar{1}]_f$ zone axis (Figure 1f).

Therefore, the reciprocal lattice of this material (Figure 2) can be represented by the reciprocal lattice of the fluorite-type cell plus a complex scattering distribution whose intensity maxima are concentrated forming rings (with the normal axis parallel to the $[111]_f$ direction) around $G_F \pm {}^1/_2(111)^*$ and equivalent positions (rings appear perpendicular to the four $[111]_f$ directions). Weaker intensity distributions are also seen as diffuse rings located at $G_F \pm (100)^*$, $G_F \pm (010)^*$ and $G_F \pm (001)^*$ positions.

The nature of the modulations giving rise to additional scattering are generally of mixed compositional and displacive character. Partial or short-range ordering of the oxygen vacancies is likely to occur in the high-temperature quenched $Y_{0.75}Nb_{0.25}O_{1.75}$. In all the fluorite-related superstructures (except the so-called C-type structure of the rare earth oxides) the anion vacancies are arranged in pairs, separated by a ${}^1/_2\langle 111\rangle_f$ lattice

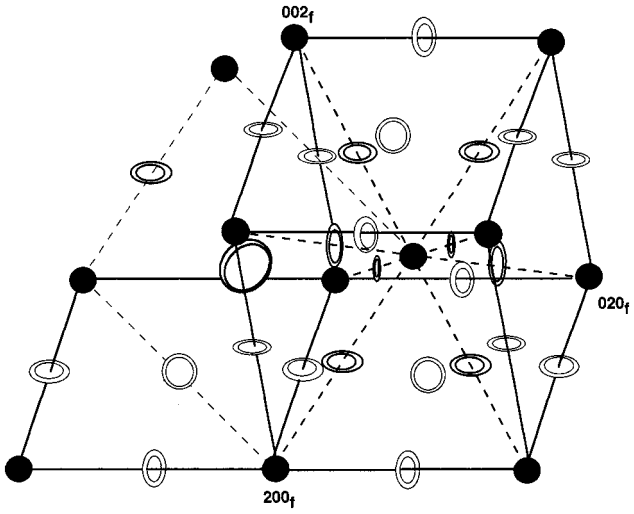

Figure 2. Drawing of the reciprocal lattice of $Y_{0.75}Nb_{0.25}O_{1.75}$ showing the diffraction effects as they are observed to occur in the electron diffraction patterns. The diffuse intensity rings around $G_F\pm(100)^*$, $G_F\pm(010)^*$, and $G_F\pm(001)^*$ are weaker than around the $G_F\pm{}^1/_2(111)^*$ positions.

vector with a cation in between.[18] In these superstructures, the cation/vacancy pair units may be isolated (as in M_7O_{12}), forming clusters (as in $CaZr_4O_9$), linked into zigzag chains along $[110]_f$ (as in the pyrochlore structure) or forming helical chains (as in $Ca_6Hf_{19}O_{44}$). In the C-type structure, the anion vacancies are arranged in pairs separated by a $^1/_2\langle 110\rangle_f$ lattice vector.

In the case of a well-ordered pyrochlore structure, besides the fluorite-type Bragg reflections, another two sets of reflections at $G_F\pm{}^1/_2(111)^*$ and $G_F\pm(001)^*$ should be observed in the diffraction patterns. In the high-temperature quenched $Y_{0.75}Nb_{0.25}O_{1.75}$, only diffuse scattering appears at these positions. Similar patterns have been observed in other fluorite-related systems such as $ZrO_2-TbO_{1.5}-GdO_{1.5}$,[9] $UO_2-CeO_{1.5}$,[10] or $ZrO_2-PrO_{1.5}$.[19,20] Van Dijk et al.[9] and Pienkowski et al.[10] explained these observations as the result of a diphasic texture of pyrochlore structure microdomains embedded in a matrix of disordered fluorite structure. However, Withers et al.[20] claimed that the extremely weak intensity of the $G_F\pm(001)^*$ reflections relative to the $G_F\pm{}^1/_2(111)^*$ scattering, rules out the possibility of this microdomain formation. They considered a commensurately compositional and displacive modulated fluorite type structure, the ordering of the ions and oxygen vacancies being in an intermediate state between those in the pyrochlore and fluorite structures.

We believe that partial oxygen-vacancy ordering similar to the one in the pyrochlore structure most likely occurs in the $Y_{0.75}Nb_{0.25}O_{1.75}$ material, but whether this partial ordering also involves the metal atoms is not yet clear. However, vacancy ordering is generally accompanied by cation ordering because a pair of vacancies implies octahedral coordination of the enclosed cation and the size of the metal ions plays an important role in their optimum location. In studies of the related Y_3TaO_7 phase by EXAFS and single-crystal X-ray diffraction, it has been suggested that the Y atoms are displaced from the ideal fluorite cation sites along $\langle 111\rangle_f$ and half of the oxygens along $\langle 001\rangle_f$.[21] Such cation displacements could well give rise to the doubling along $\langle 111\rangle$ observed for $Y_{0.75}Nb_{0.25}O_{1.75}$ in this study, however, this is best discussed in terms of the entire system, not just the end member, see below.

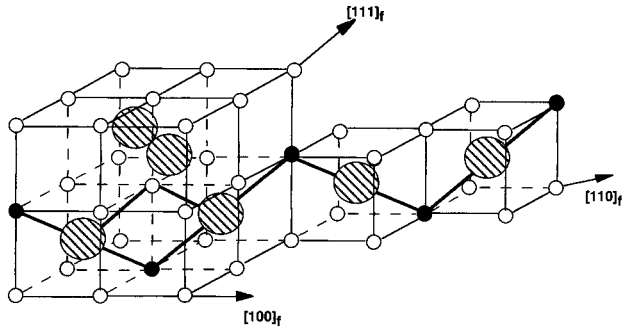

Figure 3. Diagram of a portion of a fluorite-type lattice with an anion-vacancies ordering similar to the one in the pyrochlore structure. Small open circles represent the anion array, the small black circles the vacancies and the large shaded circles the cation array. The thick lines link a pair of anion sites showing how they form a bridge between neighboring cation sites and the zigzag chains of the anion-vacancies along [110] direction.

With regard to the atomic displacement, some characteristic features can be seen in the SAED patterns. The diffuse rings are intersected by "dark lines" (see arrows in the SAED patterns along the $[\bar{1}\bar{1}2]_f$ and $[3\bar{3}2]_f$ zone axes, Figure 1) and some asymmetry in the intensity across the dark lines is observed. These effects are characteristic of atomic relaxation displacements through "size-effect-like" distortions.[22] The distortions consist of static displacements of atoms from their ideal crystallographic positions producing a strain field that is propagated outward relatively long distances along rows of atoms. Single-crystal X-ray diffraction studies on some yttria-stabilized zirconias have shown similar features,[23−25] and it was concluded from these studies that nearest neighbor $^1/_2[110]_f$ cations are further apart if one of the two bridging oxygen-atom sites is vacant or closer together if both oxygen sites are occupied (see Figure 3). An oxygen vacancy affects the four cations surrounding it, with the cations moving out from the vacancy along $[111]_f$ although the effect of this displacement will be transmitted along the $[110]_f$ rows of cations. Oxygen ion displacements were also considered in these studies. A similar kind of periodic ion displacements and subsequent distortion has been reported for Y_3TaO_7[21] and may also occur in $Y_{0.75}Nb_{0.25}O_{1.75}$, but this should be confirmed by single-crystal X-ray diffraction or neutron powder diffraction.

Figure 4 shows two HRTEM images of $Y_{0.75}Nb_{0.25}O_{1.75}$. Such images are characteristic of a partial or short-range ordered structure and do not reveal a two-phase

(18) Rossel, H. J.; Scott, H. G. *J. Phys. Colloq.* **1977**, *38*, C7−28.
(19) Withers, R. L.; Thompson, J. G.; Barlow, P. J. *J. Solid State Chem.* **1991**, *94*, 89.
(20) Withers, R. L.; Thompson, J. G.; Barlow, P. J.; Barry, J. C. *Aust. J. Chem.* **1992**, *45*, 1375.
(21) Tanaka, T.; Ishizawa, N.; Yoshimura, M.; Marumo, F.; Oyangi, H. *J. Solid State Chem.* **1995**, *114*, 79.
(22) Butler, B. D.; Withers, R. L.; Welberry, T. R. *Acta Crystallogr. A* **1992**, *48*, 737.
(23) Welberry, T. R.; Withers, R. L.; Thompson J. G.; Butler, B. D. *J. Solid State Chem.* **1992**, *100*, 71.
(24) Welberry, T. R.; Butler, B. D.; Thompson, J. G.; Withers, R. L. *J. Solid State Chem.* **1993**, *106*, 461.
(25) Welberry, T. R.; Withers, R. L.; Mayo, S. C. *J. Solid State Chem.* **1995**, *115*, 43.

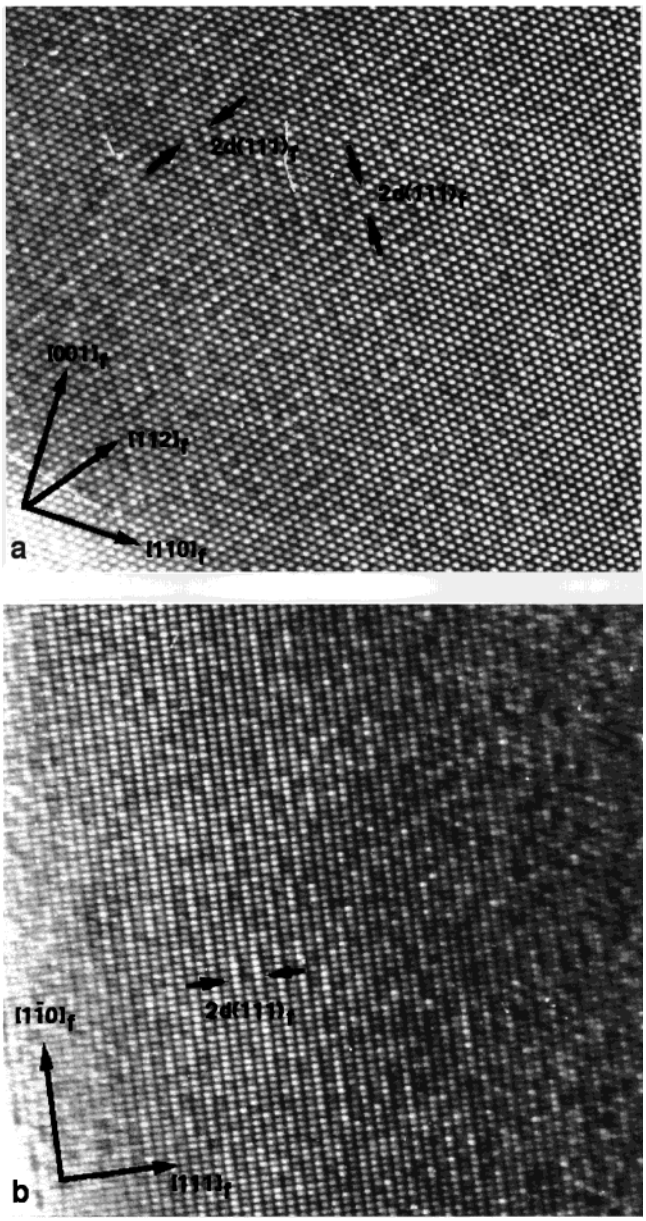

Figure 4. HRTEM images of $Y_{0.75}Nb_{0.25}O_{1.75}$ corresponding to the $[\bar{1}\bar{1}0]_f$ (a) and $[\bar{1}\bar{1}2]_f$ (b) zone axes.

situation. Lattice fringes along $[112]_f$ and $[\bar{1}\bar{1}2]_f$ directions separated by a distance corresponding to twice $d\{111\}_f$ are seen in the image along the $[\bar{1}\bar{1}0]_f$ zone axis, confirming the doubling of the average fluorite periodicity along the $[111]_f$ directions. A short-range pyrochlore-type ordering of the oxygen vacancies without the need of metal ordering considerations can explain the contrast differences in this image, as schematically represented in Figure 5. The HRTEM image belonging to the $[\bar{1}\bar{1}2]_f$ zone axis shows a brightness variation of the dots forming a modulation along $[1\bar{1}0]_f$ direction which originates a periodicity of twice $d\{111\}_f$ along the $[111]_f$ directions. This modulation should correspond to the cation/vacancy pair units forming zigzag chains through the $[110]_f$ direction doubling the average fluorite structure along $[111]_f$.

To study the evolution of the modulation with the composition in the high-temperature quenched $(1-x)$-$Y_{0.5}Zr_{0.5}O_{1.75}-xY_{0.75}Nb_{0.25}O_{1.75}$ $(0 \le x \le 1)$ oxides, we have chosen the diffraction patterns corresponding to

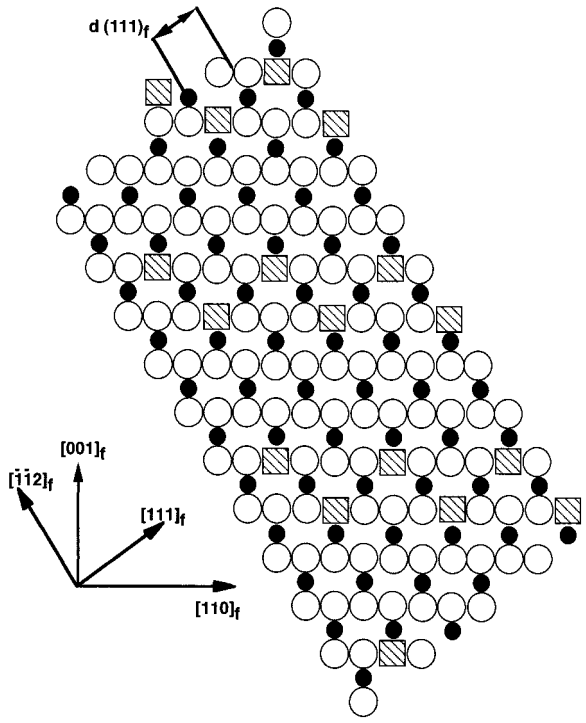

Figure 5. Schematic representation of the pyrochlore structure projected on the $(1\bar{1}0)$ plane. Small black circles represent the cations, large open circles the oxygen anions and the dashed squares the anion vacancies. The vacancies are arranged along the $[\bar{1}\bar{1}2]$ direction in a way which doubles the structure along the [111] direction.

the $[\bar{1}\bar{1}0]_f$ and $[\bar{1}\bar{1}2]_f$ zone axis because they are the most informative patterns, as the scattering distribution at $G_F \pm {}^1/_2(111)^*$ and $G_F \pm (001)^*$ can be observed simultaneously. Figure 6 shows representative SAED patterns of four samples with different composition.

All the patterns along the $[\bar{1}\bar{1}0]_f$ zone axis present a continuous square wave type of diffuse distribution. This distribution runs through $G_F \pm {}^1/_2(111)^*$ and $G_F \pm ({}^1/_4+\delta)$-$(220)^*$ positions and is also observed along the $[\bar{1}\bar{1}2]_f$ axis. The $Y_{0.5}Zr_{0.5}O_{1.75}$ oxide shows weak satellite reflections at $G_F \pm ({}^1/_4+\delta)(220)^*$; in the samples with composition $Y_{0.65}Zr_{0.2}Nb_{0.15}O_{1.75}$ and $Y_{0.575}Zr_{0.35}Nb_{0.075}O_{1.75}$, the scattering distribution condenses into two reflections at both sides of $G_F \pm {}^1/_2(111)^*$; in the patterns of $Y_{0.55}Nb_{0.05}$-$Zr_{0.4}O_{1.75}$, both types of reflections can be seen.

Suzuki et al. have studied some high-temperature quenched compounds of the $ZrO_2-Y_2O_3$ system,[26] reporting the same SAED patterns for the 40 mol % Y_2O_3 composition as we do for $Y_{0.5}Zr_{0.5}O_{1.75}$. They suggested a random mixture of two commensurate structures on the basis of displacements of the oxygen atoms. However, we interpret our SAED patterns as characteristic of a modulated structure due to compositional and displacive perturbations of the basic fluorite cell.

The $G_F \pm ({}^1/_4)(220)^*$ and $G_F \pm (001)^*$ reflections are characteristic of the C-type structure of the Ln_2O_3 oxides (Ln = lanthanide element). Therefore, a smooth transition from pyrochlore-related to C-type related structures as a function of the cationic composition seems to occur in this system. At compositions with both high yttrium and high niobium content, a partial structure ordering

(26) Suzuki, S.; Tanaka, M.; Ishigame, M. *Japanese J. Appl. Phys.* **1985**, *24* (4), 401.

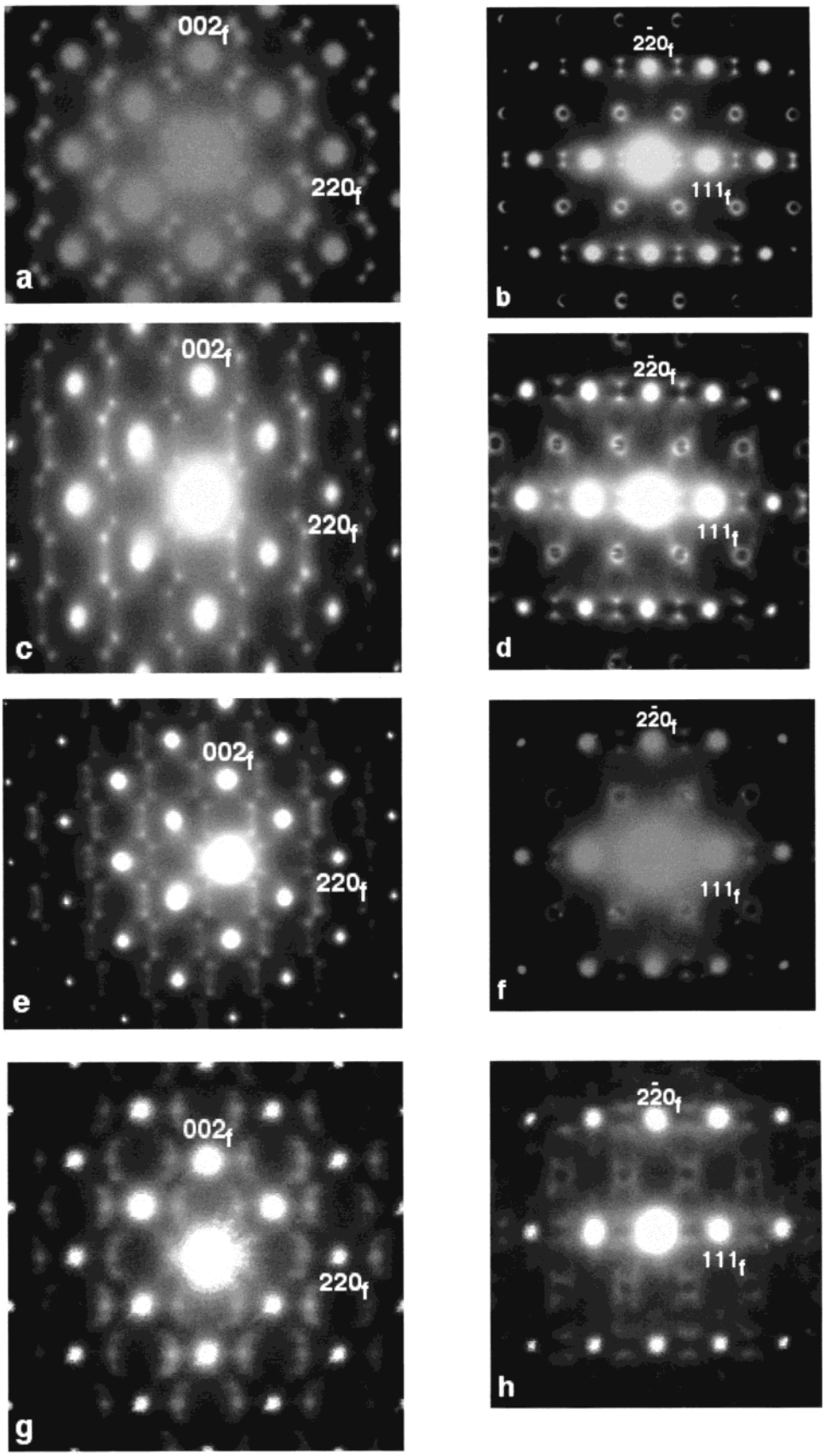

Figure 6. SAED patterns along the $[\bar{1}\bar{1}0]_f$ and $[\bar{1}\bar{1}2]_f$ zone axes of the $Y_{0.65}Zr_{0.2}Nb_{0.15}O_{1.75}$ (a and b); $Y_{0.575}Zr_{0.35}Nb_{0.075}O_{1.75}$ (c and d); $Y_{0.55}Zr_{0.4}Nb_{0.05}O_{1.75}$ (e and f), and $Y_{0.5}Zr_{0.5}O_{1.75}$ (g and h).

close to the one in the pyrochlore structure occurs. The modulation changes with the composition until an incommensurably modulated ($\delta \neq 0$) fluorite structure, due to a partial ordering related to C-type, is observed for $Y_{0.5}Zr_{0.5}O_{1.75}$. A kind of ordering intermediate between these two structures occurs at intermediate compositions. The gradual transition between the C-type and the pyrochlore structures with composition has

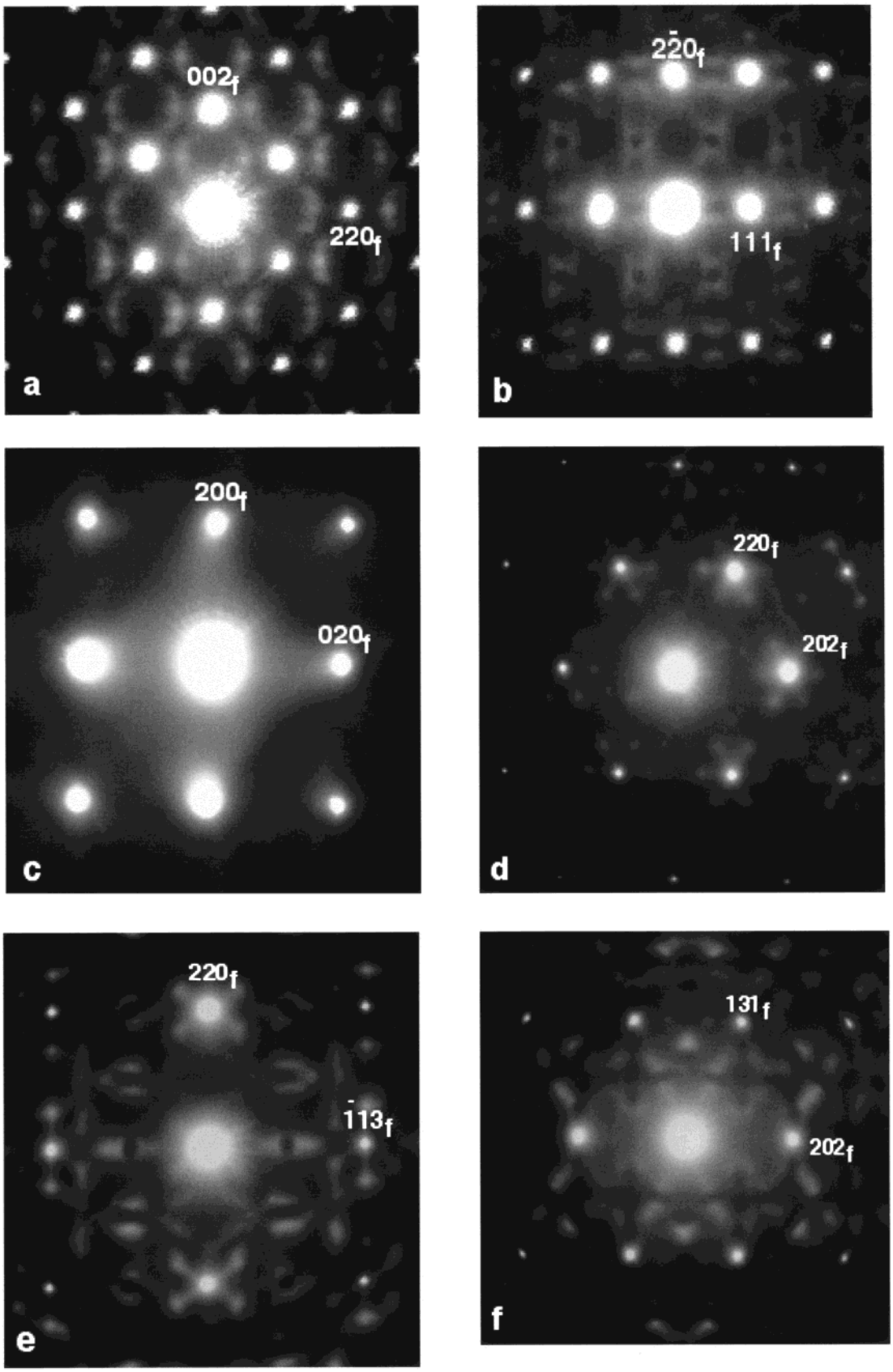

Figure 7. SAED patterns of $Y_{0.5}Zr_{0.5}O_{1.75}$ along $[\bar{1}\bar{1}0]_f$ (a), $[\bar{1}\bar{1}2]_f$ (b), $[001]_f$ (c), $[1\bar{1}\bar{1}]_f$ (d), $[3\bar{3}2]_f$ (e), and $[10\bar{1}]_f$ (f) zone axes.

also been reported in some $ZrO_2-Ln_2O_3$ (Ln = Tb, Dy, Ho) systems.[19] These kinds of "transitions" between two apparently different structures is characteristic of the so-called "structurally and compositionally flexible phases".[27] In these phases, flexibility is manifested, in reciprocal space in the form of compositionally dependent diffuse intensity distributions accompanying the strong Bragg reflections of the average structure. The pyrochlore-type modulation is the more pronounced throughout the series and it even seems to persist to

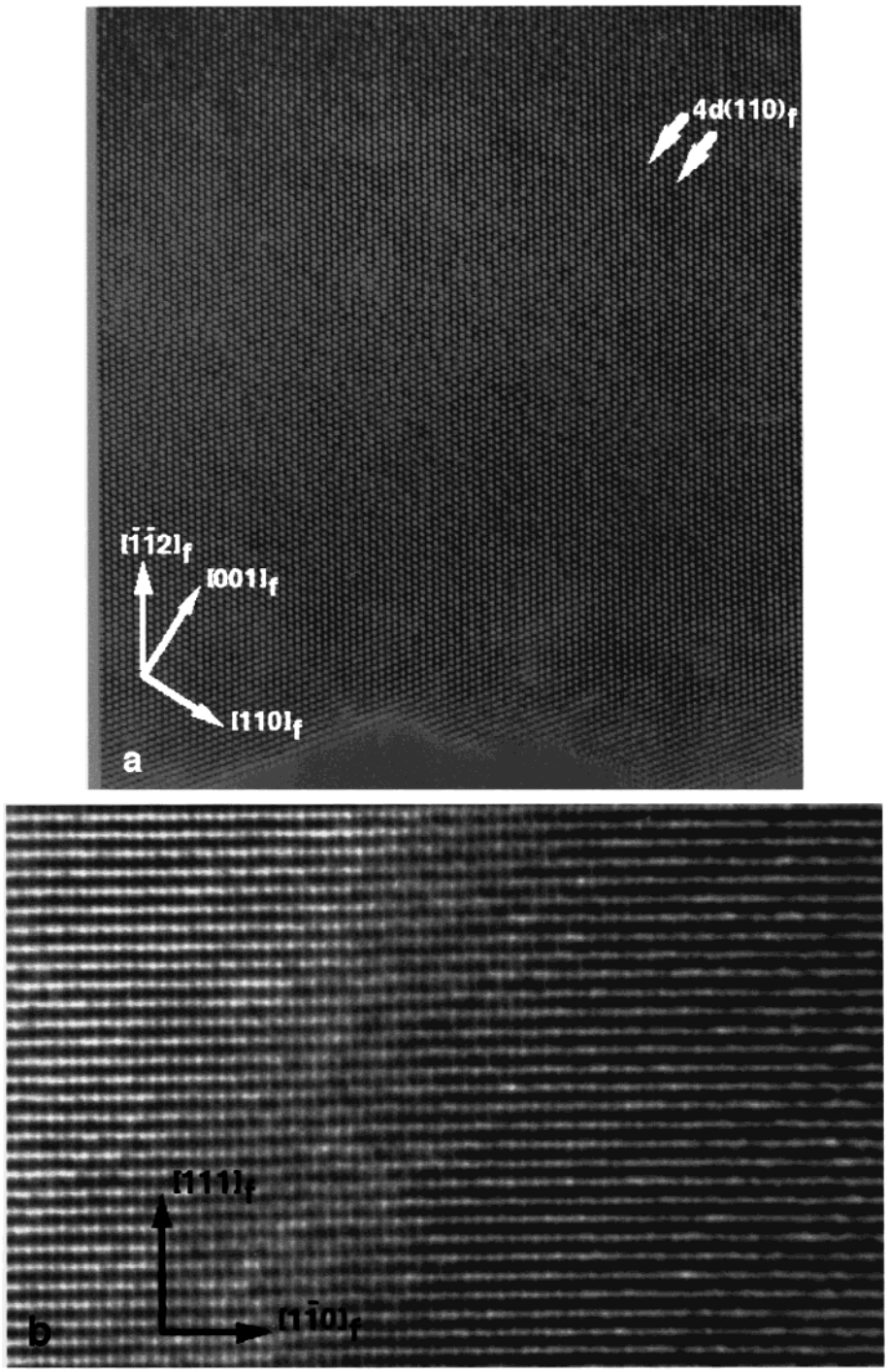

Figure 8. HRTEM images of $Y_{0.5}Zr_{0.5}O_{1.75}$ corresponding to $[\bar{1}\bar{1}0]_f$ (a) and $[\bar{1}\bar{1}2]_f$ (b) zone axes.

$Y_{0.5}Zr_{0.5}O_{1.75}$ where some indications still remain. Neutron diffraction studies on this system show that the isotropic temperature factors for the cations are almost independent of composition, apart from a slight increase for the $Y_{0.75}Nb_{0.25}O_{1.75}$ end member; however, the anionic values are much larger and increase linearly with the Nb content.[15] As the pyrochlore type modulation features similarly increase in magnitude with the Nb content, it seems that the distortions in the anion sublattice play a greater role than cationic distortions, such as those reported for Y_3TaO_7,[21] in driving the pyrochlore-type modulation.

We will now give a more detailed description of the reciprocal lattice of the $Y_{0.5}Zr_{0.5}O_{1.75}$ material. Figure 7 shows representative SAED patterns along different zone axes of this compound. The patterns present a complex scattering distribution. Weak satellite reflections at $G_F \pm (1/4 + \delta)(220)^*$ and equivalent positions are observed. However, the $G_F \pm (001)^*$ reflections, which are the second set of satellite reflections characteristic of the C-type structure, do not appear. Some diffuse scattering around $G_F \pm 1/2(111)^*$ still remains, although

(27) Withers, R. L.; Schmid, S.; Thompson, J. G. *Prog. Solid State Chem.* **1998**, *26*(1).

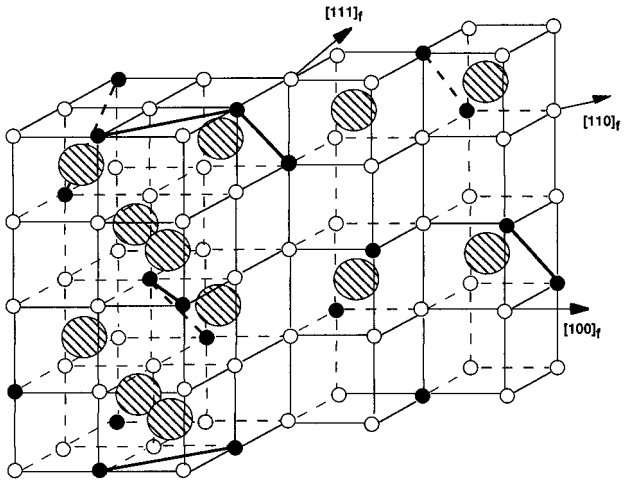

Figure 9. Diagram of a portion of the C-type structure of Ln_2O_3 (Ln = rare earth element). Small open circles represent the oxygen array; the small black circles, the oxygen vacancies; and the large shaded circles, the cation array.

its shape is different from that observed in the patterns of the other samples (the two reflections at both sides of $G_F \pm 1/2(111)$* are now long rows).

The absence of $G_F \pm (001)$* type satellite reflections seems to be due to characteristic satellite extinction conditions of modulations associated with specific irreducible representations. The irreducible representation consistent with the lack of existence of $G_F \pm (001)$* type reflections is related to compositional modulation due to C-type oxygen-vacancy ordering but does not allow metal atom ordering.[28] Therefore, an oxygen-vacancy ordering close to the C-type structure is most likely to be occurring in the high-temperature quenched $Y_{0.5}Zr_{0.5}O_{1.75}$. However, the complete transition from the pyrochlore-related to the C-type ordering has not yet been achieved in this material. An intermediate vacancy ordering between the two structures is established, although it is closer to the C-type than to the pyrochlore structure. "Dark-lines" and a certain asymmetry in the intensity across the "dark-lines" associated with atomic displacements are also observed in the patterns of Figure 7.

Figure 8 shows two HRTEM images of $Y_{0.5}Zr_{0.5}O_{1.75}$ which again do not reveal a phase-mixture texture. In the image corresponding to the $[\bar{1}\bar{1}0]_f$ zone axis, an average fluorite lattice is clearly visible but a very weak modulation along $[\bar{1}\bar{1}2]_f$ can be observed, giving rise to fringes parallel to $[001]_f$. These fringes seem to be separated about four times $d\{110\}_f$ in some parts of the crystal, in agreement with the oxygen-vacancy distribution in the C-type structure (see Figure 9). The image along the $[\bar{1}\bar{1}2]_f$ zone axis shows, mainly in the thick parts of the crystal, a contrast modulation along the $[1\bar{1}0]_f$ direction. The modulation must be due to the oxygen-vacancy ordering along this direction. Pyrochlore-related doubling of the average structure along $[111]_f$ is not found either in the image along the $[\bar{1}\bar{1}0]_f$ zone axis nor in the image along the $[\bar{1}\bar{1}2]_f$ one, despite the weak diffuse intensity distribution around $G_F \pm 1/2(111)$* observed in the SAED patterns.

In fluorite-related structures, vacancies are typically incorporated as 6-fold coordination on one cation site. In a pyrochlore such as $Gd_2Ti_2O_7$, the large Gd ion is normally considered to be in 8-fold coordination and the small Ti ion in 6-fold coordination. In $Gd_2Zr_2O_7$ a similar pyrochlore-type order can be sustained; however, in $Y_2Zr_2O_7$, the size difference between Y and Zr is no longer sufficient to drive long-range pyrochlore-type order and so short-range order of C-type is principally observed. In the ideal C-type structure, all cations adopt 6-fold coordination. As Y + Nb replaces 2Zr in the $(1-x)Y_{0.5}Zr_{0.5}O_{1.75}-xY_{0.75}Nb_{0.25}O_{1.75}$ system, the Nb ion, which is slightly smaller than Zr, might be expected to enhance pyrochlore-type order due to the bigger size difference with yttrium. On the other hand, the move from $A_2B_2O_7$ to A_3BO_7 stoichiometry might be expected to mitigate against pyrochlore type order. In this study, we have shown that pyrochlore type order dominates as Nb is introduced into the structure.

The role of ion size is questioned by the results of EXAFS studies on the Y_3TaO_7 phase,[21] which suggest that, in this phase, the smaller ion, Ta has a larger coordination number and that the larger ion, Y has a smaller coordination number. As it is now generally accepted that the vacancies in yttria-stabilized zirconia are associated with the smaller Zr ion, further investigation of the coordination environments in this $(1-x)$-$Y_{0.5}Zr_{0.5}O_{1.75}-xY_{0.75}Nb_{0.25}O_{1.75}$ system would significantly add to this debate.

Conclusions

Electron diffraction and microscopy studies indicate that the high-temperature quenched oxides of the $(1-x)Y_{0.5}Zr_{0.5}O_{1.75}-xY_{0.75}Nb_{0.25}O_{1.75}$ ($0 \le x \le 1$) system have a modulated fluorite-type structure. Anion vacancies are not isolated or randomly distributed within the structure of these materials.

The modulation of the structure in $Y_{0.75}Nb_{0.25}O_{1.75}$ is associated with a partial or short-range pyrochlore-related ordering of the oxygen vacancies. Whether this ordering also involves metal ions is not yet clear although it is likely.

A smooth transition from pyrochlore-related to C-type-related ordering as a function of the composition (with the yttrium and niobium content decreasing) is observed. In this way, $Y_{0.5}Zr_{0.5}O_{1.75}$ presents an incommensurably modulated fluorite structure, which essentially suggests a partial C-type-related ordering of the oxygen vacancies, but metal ordering seems not to occur. The modulation of the structure of these materials is also associated with ion displacements away from their crystallographic positions. Therefore, the $(1-x)$-$Y_{0.5}Zr_{0.5}O_{1.75}-xY_{0.75}Nb_{0.25}O_{1.75}$ ($0 \le x \le 1$) oxides are "structurally and compositionally flexible phases".

As the ionic conductivity decreases with increasing yttrium and niobium content it appears that pyrochlore-related ordering is less favorable for the anion mobility than C-type-related ordering.

Acknowledgment. Authors thank CICYT (MAT 98-1053) for financial support and the Microscopy Centre Luis Bru from U.C.M. for technical assistance. We also thank the EPSRC and the Royal Society of Edinburgh for financial support.

CM991204L

(28) Withers, R. L.; Wallenberg, R.; Bevan, D. J. M.; Thompson, J. G.; Hyde, B. G. *J. Less-Common Met.* **1989**, *156*, 17.